Available online at www.sciencedirect.com
SCIENCE DIRECT
Journal of Sound and Vibration 295 (2006) 890–905
JOURNAL OF SOUND AND VIBRATION
www.elsevier.com/locate/jsvi

Simulation on the motion of crankshaft with crack in crankpin-web fillet region

Xuanyang Lei[a,*], Guicai Zhang[a], Song Xigeng[b], Jin Chen[a], Guangming Dong[a]

[a]*State Key Laboratory of Vibration, Shock and Noise, Shanghai Jiao Tong University, Shanghai 200030, PR China*
[b]*Institute of Internal Combustion Engine, Dalian University of Technology, Dalian 116023, PR China*

Received 22 October 2004; received in revised form 14 June 2005; accepted 27 January 2006
Available online 2 May 2006

Abstract

A new method for simulating nonlinear motion of cracked crankshaft is proposed, and the transient vibration response of a cracked crankshaft is evaluated and analyzed. First, the crankshaft without crack is simplified as a finite element model based on spatial *Timoshenko* beam element, and the vibration modes of the crankshaft are calculated and compared with the results presented in other published literatures. Then, the frequently occurred crack in crankpin-web fillet region is studied. According to the characteristic of this kind of crack, a new spatial crack beam element is developed, and a cracked crankshaft model, which combines crack beam element and *Timoshenko* beam elements, is established. Subsequently, the breathing behavior of the crack under operating condition is discussed, and the nonlinear equation of motion of cracked crankshaft is set up. Finally, the transient vibration response of the cracked crankshaft under fire condition is evaluated, and the influence of the crack depth on the vibration response of torsion, translation and bending are analyzed. The modeling and analysis procedures are applied to a crankshaft system of a four in-line cylinder engine. This investigation provides a useful tool for the vibration analysis and crack detection of cracked crankshaft system.

1. Introduction

The crack in crankshaft is one of the most frequently occurred faults for Internal Combustion Engines. According to a survey on the shipwreck during 1976–1980 in Japan, 18.6% of the causes is the crankshaft broken [1]. Many researchers have investigated the dominant mechanism, causation, and extension of the crack in crankshaft surface, or the life prediction for crankshaft. Pandey [2] investigated the dominant mechanism of failure of crankshafts, and estimated the stress level required for fatigue initiation and propagation from the crankpin-web fillet region. Sofronas [3] analyzed and determined the causation for failed crankshaft in a single-engine aircraft. Taylor [4] predicted the fatigue limit for a crankshaft by using a technique of crack modeling. Guagliano [5] studied the crack propagation in a crankshaft. Miyahara [6] predicted the fatigue crack initiation and propagation lives in a crankshaft quantitatively. Wang [7] studied the diagnosis of crankshaft cracks via the measurement of the torsional modal characters of an imitated crankshaft flywheel system. To simulate the vibration behavior of crankshaft, many models including

*Corresponding author.
E-mail addresses: leixy@sjtu.edu.cn (X.Y. Lei), gczhang@sjtu.edu.cn (G. Zhang), jinchen@mail.sjtu.edu.cn (J. Chen).

0022-460X/$ - see front matter © 2006 Elsevier Ltd. All rights reserved.
doi:10.1016/j.jsv.2006.01.044

equivalent system, simply supported beam, spatial rigid frame and solid finite element are used in previous work [8–13]. It is evident that the solid finite element model in 3-D is the most competent one; however, it is computationally expensive to simulate the transient vibration and nonlinear vibration of a crankshaft system. The simply supported beam model is of little exactness due to its immoderate simplicity. The spatial rigid frame model combined with the method of dynamic stiffness matrix, transfer matrix and the finite element based on Euler–Bernulli beam theory were applied to analyze the dynamic behavior of the crankshaft in Refs. [10–12], respectively. However, the results showed that a large difference existed between the experimental and analytical value of certain modes.

It is evident that the spatial rigid frame model is simplified and computationally effective for vibration analysis of crankshaft system. Though the discrete components of crankshaft are not slender beams, Refs. [13–15] indicated that the *Timoshenko* beam elements including rotary inertia and the shear deformation could improve the accurateness of analytical results (especially for higher modes). Therefore, it is proposed to establish a finite element model for vibration analysis of crankshaft system by applying a 3-node spatial *Timoshenko* beam element in this work. Moreover, the engine block stiffness is idealized as a pair of vertical and horizontal linear springs for each main bearing, and the other parts are simplified as equivalent mass elements. In order to exhibit effectiveness of the proposed model, the frequencies of a crankshaft are determined and compared with the results presented in Refs. [10,13].

Because of fatigue and stress concentration, crack occurs most frequently in the crankpin-web fillet region for crankshaft. Generally, this crack will be transverse, 45° to the cross-section and at the surface of crank web [4,16]. According to the case, a corresponding slant crack beam element is proposed to model the crank web with such kind of crack. It is well known that the presence of a transverse crack in a structure member would introduce local flexibility, which for a beam can be described by a local flexibility matrix [17]. Such theory is widely used in many open literatures for the dynamic analysis of crack beam, shaft and rotor [17–21]. Based on the theory, the stiffness of the beam element with slant crack is developed in this study. Thereupon, a new model for cracked crankshaft is established by combining the developed slant crack beam element and the 3-node *Timoshenko* beam elements mentioned above. In order to validate the developed slant crack beam element and the method for cracked crankshaft model, the frequencies of a cracked single cylinder crankshaft are evaluated numerically by using beam elements and solid elements, respectively, and the results are compared with each other.

In order to simulate the motion of the crankshaft, the support provided by engine block is considered, and the rotating crankshaft and the non-rotating engine block are combined in a rotating coordinate system. Furthermore, the breathing behavior of crack is studied, and the nonlinear motion equation for cracked crankshaft system is set up. The crankshaft of a four in-line cylinder engine provided in Ref. [12] is applied as an example, and a slant crack is presumed in one of the crankpin-web fillet region. The current modeling method is implemented, the motion of the crankshaft with or without crack is simulated, and the influence of crack depth on the transient response of operating crankshaft is analyzed.

2. 3-node Timoshenko beam element

The 3-node Timoshenko beam element applied in this paper is a quadratic beam element in 3-D (as in Fig. 1), and has six degrees of freedom at each node, these include translations (u, v, w) in the x, y, and z directions and rotations (θ_x, θ_y. θ_z) about the x, y, and z directions . It is an element including shear deformation and rotary inertia effects and suitable for analyzing slender to moderately stubby and thick beam structures.

The shape function of the 3-node element is

$$N_i = \tfrac{1}{2}\eta(\eta-1), \quad N_j = \tfrac{1}{2}\eta(\eta+1), \quad N_k = 1-\eta^2, \tag{1}$$

where η is the nature coordinate ($-1 \leqslant \eta \leqslant 1$).

The displacement at a generic point p on the element is expressed in a vector form as $\{\delta_p\} = [\,u_p \quad v_p \quad w_p \quad \theta_{xp} \quad \theta_{yp} \quad \theta_{zp}\,]^{\mathrm{T}}$. Then the displacement of point p is related to the element nodal displacements $\{\delta_i\}$, $\{\delta_y\}$ and $\{\delta_k\}$ by

$$\{\delta_p\} = N_i \cdot \{\delta_i\} + N_j \cdot \{\delta_j\} + N_k \cdot \{\delta_k\}, \tag{2}$$

$\{\delta_i\}$, $\{\delta_j\}$, $\{\delta_k\}$ is the vector of displacement at nodes i, j and k respectively.

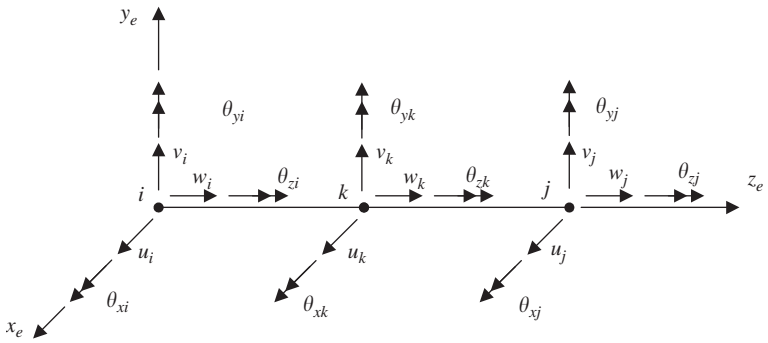

Fig. 1. The 3-node Timoshenko beam element.

3. Modeling for crankshaft-bearing system

For comparison purpose, the crankshaft-bearing system of a 4 in-line cylinder engine provided in Refs. [10,13] is applied in this study. The system includes crankshaft body, front pulley, flywheel and main bearing. The current 3-node Timoshenko beam element is applied to establish a valid model for the vibration behavior of the crankshaft. The modeling procedure is now summarized.

3.1. Crankshaft body

In the crankshaft body, the shaft members of five main journals, four crankpins, and the front pulley end and flywheel end are represented by a spatial round 3-node Timoshenko beam element of appropriate diameters. Each of the 3 central main journals is divided into 2 elements. Each of the end journals, flywheel, and front pulley ends is considered as a single element. Each cheek is divided into 3 sections as Ref. [13], and every section is represented by a spatial rectangular 3-node Timoshenko beam element. The finite element model of overall crankshaft body is shown in Fig. 2. There are 38 elements and 77 nodes in total. Only the initial and terminal nodes of each element are shown. The dimensional parameters of the elements are listed in Table 1.

3.2. Front pulley and flywheel

The front pulley and flywheel are idealized by a set of masses and mass moments of inertia about 3 orthogonal axes attached at the end nodes of the corresponding elements, i.e., the front pulley at node 1 and the flywheel at node 77 with masses and moments of inertia given in Table 2.

3.3. Crankshaft main bearings

Each of the main bearings is idealized according to Ref. [10]. The oil film of each journal bearing is idealized by a set of equivalent linear spring and dashpots in the vertical and horizontal direction, i.e. the y and z direction in Fig. 2. The linear spring and dashpots elements are attached at the node in the middle of each bearing. The stiffness of the equivalent linear spring attached at two end journal (1# and 5#) is $k^{\mathrm{I}}_{yy} = k^{\mathrm{I}}_{zz} = 8 \times 10^8$ N/m, and the stiffness of the equivalent linear spring attached at three central journal (2#, 3# and 4#) is $k^{\mathrm{I}}_{yy} = k^{\mathrm{I}}_{zz} = 9 \times 10^9$ N/m.

3.4. Piston and connection rod

The equivalent mass of the piston and connecting rod are idealized as a set of lumped masses at the end nodes of a crankpin element. The equivalent mass is given in Ref. [13] is used, and $m = 1.8$ kg. This equivalent

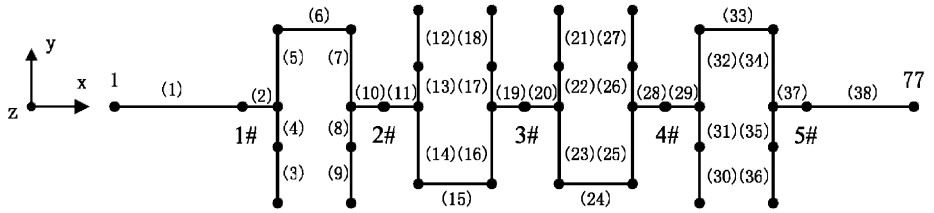

Fig. 2. The finite element model of the crankshaft body.

Table 1
Element dimensions and the members they represent in Fig. 2

Element	Dimension (mm)
1	$\phi 48 \times 72$
2, 10, 11, 19, 20, 28, 29, 37	$\phi 48 \times 21.75$
5, 7, 14, 16, 23, 25, 32, 35	$70 \times 19.5 \times 41$
4, 8, 13, 17.22, 26, 31, 35	$73 \times 14 \times 36$
3, 9, 12, 18, 21, 27, 30, 36	$84 \times 13 \times 29$
6, 15, 24, 33	$\phi 46 \times 43.5$
38	$\phi 48 \times 35.5$

Table 2
Mass properties of front pulley and flywheel

	M (kg)	I_{xx} (kg m^2)	I_{yy} (kg m^2)	I_{zz} (kg m^2)
Front pulley	2.01	6.38×10^{-3}	3.65×10^{-3}	3.65×10^{-3}
Flywheel	10.15	0.15	0.075	0.075

mass is divided equally into two parts attached at each end of the crankpin. Thus, a lumped mass of 0.9 kg has been considered at all translational freedoms at two end nodes of elements 6, 15, 24 and 33.

4. Results and discussion

Subspace iteration is used to evaluate the modes of the finite element model of the 4-cylinder engine crankshaft established in Section 3. The evaluated and experimental results of the first 8 orders natural frequencies and the modes are listed in Table 3. For comparison, the corresponding results presented in Refs. [10,13] are listed in the table too. In Table 3, "I" refers to the vibration deformation in x–y plane, and "O" refers to the vibration deformation in x–z plane of Fig. 2.

It can be seen from the results presented in Table 3 that:

(1) The 1st and 5th order natural frequency simulated using 3-node spatial *Timoshenko* beam element is the most approximate to the experimental value (the experimental result of second mode is not given in Refs. [10,13]). The error of the first order in our study is 5.6%, whereas it is 16.5% in Ref. [10].
(2) The 5th and 6th mode shapes are consistent with the experimental results, and the results of Ref. [13] are not consistent with the experimental results.
(3) To the 7th and the 8th mode, the frequencies evaluated are not exact and the mode shapes are not consistent with the experimental results. The same case exists in Refs. [10,13] too. This problem was investigated in Ref. [22], and a conclusion is drawn that the causation is simplifying the flywheel as a

Table 3
Comparison of the natural frequencies (Hz) obtained by different methods

Orders	Results of Ref. [10]	Results of Ref. [13]	Current results	Experimental results
1	223.0(I)	225.5(I)	254.37(I)	267.0(I)
2	255.0(O)	334.4(O)	257.84(O)	—
3	393.0(O)	383.6(O)	354.37(O)	410.0(O)
4	424.0(I)	445.3(I)	504.99(I)	440.0(I)
5	478.0(O)	561.0(I)	536.87(O)	542.0(O)
6	540.0(I)	691.2(O)	635.12(I)	542.0(I)
7	639.0(O)	1000.0(O)	926.53(O)	619.0(I)
8	669.0(I)	1000.6(I)	1088.40(I)	658.0(O)

lumped mass. When the flywheel is meshed by solid elements, the accuracy of the first 10 order mode frequencies will be improved, and the mode shapes will be consistent with that of the experiments.

Though the third and fourth natural frequencies predicted by current model have more errors than those of Refs. [10,13], the results and discussion indicate that the finite element model about crankshaft based on the spatial *Timoshenko* beam element is effective.

5. Modeling for the cracked crankshaft

In Sections 3 and 4, a finite element model was proposed to simulate the vibration behavior of the crankshaft. In this section, we will build a cracked crankshaft model based on the success of previous sections.

5.1. The cracked crankshaft model

Under the firing condition, crankshaft is endured an alternative impulsion load. The magnitude of stress in the crankpin-web fillet region will change periodically with a great extent, and then the damage with fatigue crack occurs frequently in this region. Generally, the crack occurs between the main journal and the crankpin, and it is transverse, 45° to the cross-section and at the surface of crank web [16] (see Fig. 3).

For the crack in the crankpin-web fillet region extends from the surface into the crank web and does not extend to other part of the crankshaft. It is proposed to represent the cracked crank web by a 2-node slant crack beam element and simplify the other parts of the crankshaft as the method described in Section 3. Comparing with the model shown in Fig. 2, the cracked model consists of the same number of elements, and the number of the nodes will be cut down according to the number of the crack beam elements representing cracked crank web. The approach for developing the stiffness of the 2-node slant cracked element will be described as follows.

5.2. 2-node spatial beam element with slant surface crack

Several approaches can be used to develop the stiffness of the crack beam element. Refs. [17,20] estimated the stiffness of a cracked rotor by introducing a local flexibility matrix. Ref. [23] represented the cracked section by a spring to model a simply supported beam. In this study, the stress intensity factors presented in Ref. [24] are applied and a new beam element with 45° slant surface crack is developed.

Consider a rectangular cross-section beam with given stiffness properties, the width and the height of the cross-section are w and h, respectively. The depth of the slant transverse crack is α and the angle towards the cross-section of the beam is 45° (see Fig. 4). The beam is loaded with axial force P_1, shear forces P_2 and P_3, bending moments P_4 and P_5, and torsional P_6. The dimension of the local flexibility matrix depends on the numbers of freedom (each node has six degrees of freedom), here is 6×6. The crack is assumed to affect only the beam stiffness and do not affect the mass distribution (still be same as that of the 2-node Euler–Bernoulli beam element), the stiffness matrix can be calculated as follows.

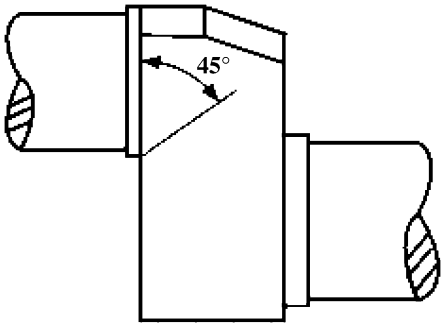

Fig. 3. The crack in crankpin-web fillet region.

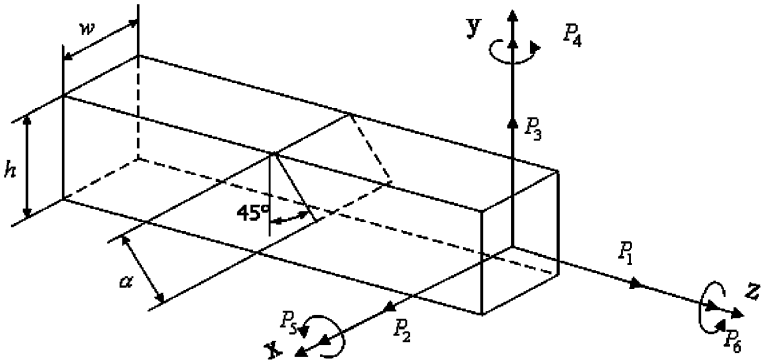

Fig. 4. A crack beam element in general loading.

Paris' equation [17] gives the additional displacement μ_i due to a crack of depth α, in the i direction, as

$$\mu_i = \frac{\partial}{\partial P_i}\left[\int_0^{\alpha} J(\alpha)\,\mathrm{d}\alpha\right], \tag{3}$$

where $J(\alpha)$ is the Strain Energy Density Function (SEDF) and P_i is the corresponding load. The SEDF is defined by

$$J = \frac{1}{E'}\left[\left(\sum_{i=1}^{6} K_{\mathrm{I}\,i}\right)^2 + \left(\sum_{i=1}^{6} K_{\mathrm{II}\,i}\right)^2 + m\left(\sum_{i=1}^{6} K_{\mathrm{III}\,i}\right)^2\right], \tag{4}$$

where $E' = E$ for plane stress or $E' = E/(1-v^2)$ for plane strain, E is the modulus of elasticity, $m = 1+v$, v is the Poisson ratio ($v = 0.3$ for steel) and K_{ij} ($i = \mathrm{I}, \mathrm{II}, \mathrm{III}$; $j = 1, 2, \ldots, 6$) are the crack Stress intensity Factors (SIF).

Then the local flexibility due to crack per unit width is

$$c_{ij}^{\mathrm{d}x} = \frac{\partial \mu_i}{\partial P_j} = \frac{\partial^2}{\partial P_i\,\partial P_j}\left[\int_0^{\alpha} J(\alpha)\,\mathrm{d}\alpha\right]. \tag{5}$$

Then integrated along the width of the crack, we have

$$c_{ij} = \frac{\partial \mu_i}{\partial P_j} = \frac{\partial^2}{\partial P_i\,\partial P_j}\left[\int_0^{w}\int_0^{\alpha} J(\alpha)\,\mathrm{d}\alpha\,\mathrm{d}x\right] = \frac{\partial^2}{\partial P_i\,\partial P_j}\left[w\int_0^{\alpha} J(\alpha)\,\mathrm{d}\alpha\right]. \tag{6}$$

According to material mechanics and fracture mechanics theory, the distribution of bending stress and shear stress introduced by torsion in the slant rectangular section is nonlinear. In order to mitigate the

complexity, the distribution is moderately simplified to be linear in this study. Thus the stress intensity factors for a strip of unit thickness with 45° slant crack are:

$$K_{\mathrm{I}1} = \sigma_{1\mathrm{I}}\sqrt{\pi\alpha}F_1(s), \quad \sigma_{1\mathrm{I}} = P_1/(2wh),$$

$$K_{\mathrm{I}3} = \sigma_{3\mathrm{I}}\sqrt{\pi\alpha}F_{II}(s), \quad \sigma_{3\mathrm{I}} = -P_3/wh,$$

$$K_{\mathrm{I}4} = \sigma_{4\mathrm{I}}\sqrt{\pi\alpha}F_1(s), \quad \sigma_{4\mathrm{I}} = (3P_4/(2w^3h))x,$$

$$K_{\mathrm{I}5} = \sigma_{5\mathrm{I}}\sqrt{\pi\alpha}F_2(s), \quad \sigma_{5\mathrm{I}} = 3P_5/(wh^2),$$

$$K_{\mathrm{I}6} = \sigma_{6\mathrm{I}}\sqrt{\pi\alpha}F_1(s), \quad \sigma_{6\mathrm{I}} = -P_6x/(\alpha'\xi w^2h^2),\ (w \geqslant \sqrt{2}h), \quad \sigma_{6\mathrm{I}} = -P_6x/(\alpha' w^3h),\ (w < \sqrt{2}h),$$

$$K_{\mathrm{II}1} = \sigma_{1\mathrm{II}}\sqrt{\pi\alpha}F_{\mathrm{II}}(s), \quad \sigma_{1\mathrm{II}} = P_1/(2wh),$$

$$K_{\mathrm{II}3} = \sigma_{3\mathrm{II}}\sqrt{\pi\alpha}F_1(s), \quad \sigma_{3\mathrm{II}} = -P_3/(wh),$$

$$K_{\mathrm{II}4} = \sigma_{4\mathrm{II}}\sqrt{\pi\alpha}F_{\mathrm{II}}(s), \quad \sigma_{4\mathrm{II}} = (3P_4/(2w^3h))x,$$

$$K_{\mathrm{II}5} = \sigma_{5\mathrm{II}}\sqrt{\pi\alpha}F_{\mathrm{II}}(s), \quad \sigma_{5\mathrm{II}} = 3P_5/(wh^2),$$

$$K_{\mathrm{III}2} = \sigma_{2\mathrm{III}}\sqrt{\pi\alpha}F_{\mathrm{III}}(s), \quad \sigma_{2\mathrm{III}} = \sqrt{2}P_2/(2wh),$$

$$K_{\mathrm{III}6} = \sigma_{6\mathrm{III}}\sqrt{\pi\alpha}F_{\mathrm{III}}(s), \quad \sigma_{6\mathrm{III}} = \sqrt{2}P_6/(4\alpha' wh^2),\ (w \geqslant \sqrt{2}h), \quad \sigma_{6\mathrm{III}} = \sqrt{2}P_6/(4\xi w^2h),\ (w < \sqrt{2}h),$$

$$K_{\mathrm{I}2} = K_{\mathrm{II}2} = K_{\mathrm{II}3} = K_{\mathrm{II}6} = K_{\mathrm{III}1} = K_{\mathrm{III}3} = K_{III4} = K_{\mathrm{III}5} = 0, \tag{7}$$

where

$$F_1(s) = \sqrt{\frac{2}{\pi s}\tan\frac{\pi s}{2}}\,\frac{0.752 + 2.02s + 0.37\left(1 - \sin\frac{\pi s}{2}\right)^3}{\cos\frac{\pi s}{2}}, \quad F_2(s) = \sqrt{\frac{2}{\pi s}\tan\frac{\pi s}{2}}\,\frac{0.923 + 0.199\left(1 - \sin\frac{\pi s}{2}\right)^4}{\cos\frac{\pi s}{2}},$$

$$F_{\mathrm{II}}(s) = \frac{1.122 - 0.561s + 0.085s^2 + 0.180s^3}{\sqrt{1-s}}, \quad F_{\mathrm{III}}(s) = \sqrt{\frac{2}{\pi s}\tan\frac{\pi s}{2}}, \quad s = \sqrt{2}\alpha/(2h),$$

$\alpha'$and ξ are the free torsional coefficient of the rectangle cross-section beam, its evaluation has relation to w/h, which is listed in Table 4.

Combining relations of Eqs. (4), (6) and (7) yields the elements of the local flexibility matrix $\overline{C}$ due to the slant crack $\overline{c}_{ij}$ $(i,j = 1, 2, \ldots, 6)$:

$$\overline{c}_{11} = \frac{\pi}{E'w}\int_0^{\overline{\alpha}} sF_1^2(s)\,\mathrm{d}s,$$

$$\overline{c}_{13} = \overline{c}_{31} = \frac{-\pi}{E'w}\int_0^{\overline{\alpha}} sF_1(s)F_{\mathrm{II}}(s)\,\mathrm{d}s,$$

$$\overline{c}_{14} = \overline{c}_{41} = \frac{6\pi}{E'w^2}\int_0^{\overline{\alpha}}\int_0^{1/2} \overline{x}sF_1^2(s)\,\mathrm{d}\overline{x}\,\mathrm{d}s,$$

$$\overline{c}_{15} = \overline{c}_{51} = \frac{6\pi}{E'A}\int_0^{\overline{\alpha}} sF_1(s)F_2(s)\,\mathrm{d}s,$$

Table 4
The evaluation of the coefficients α' and ξ related to h/w

h/w	1.00	1.20	1.50	1.75	2.00	2.50	3.0	4.0	5.0	6.0	8.0	10.0	∞
α'	0.208	0.219	0.231	0.239	0.246	0.258	0.267	0.282	0.291	0.299	0.307	0.313	0.333
ξ	1.00	0.93	0.86	0.80	0.77	0.75	0.74	0.74	0.74	0.74	0.74	0.74	0.74

$$\overline{c}_{16}=\overline{c}_{61}=\begin{cases}\dfrac{-2\pi}{E'\alpha' A}\int_0^{\overline{\alpha}}\int_0^{1/2}\overline{x}sF_1(s)F_{\mathrm{II}}(s)\,\mathrm{d}\overline{x}\,\mathrm{d}s & (w\geqslant\sqrt{2}h),\\ \dfrac{-2\pi}{E'\alpha'\xi w^2}\int_0^{\overline{\alpha}}\int_0^{1/2}\overline{x}sF_1(s)F_{\mathrm{II}}(s)\,\mathrm{d}\overline{x}\,\mathrm{d}s & (w<\sqrt{2}h),\end{cases}$$

$$\overline{c}_{22}=\frac{\pi m}{E'w}\int_0^{\overline{\alpha}}sF_{\mathrm{III}}^2(s)\,\mathrm{d}s,$$

$$\overline{c}_{26}=\overline{c}_{62}=\begin{cases}\dfrac{\pi m}{2E'\alpha' A}\int_0^{\overline{\alpha}}sF_{\mathrm{III}}^2(s)\,\mathrm{d}s & (w\geqslant\sqrt{2}h),\\ \dfrac{\pi m}{2E'\alpha'\xi w^2}\int_0^{\overline{\alpha}}sF_{\mathrm{III}}^2(s)\,\mathrm{d}s & (w<\sqrt{2}h),\end{cases}$$

$$\overline{c}_{33}=\frac{\pi}{E'w}\int_0^{\overline{\alpha}}sF_{\mathrm{II}}^2(s)\,\mathrm{d}s,$$

$$\overline{c}_{34}=\overline{c}_{43}=-\frac{6\pi}{E'w^2}\int_0^{\overline{\alpha}}\int_0^{1/2}\overline{x}sF_1(s)F_{\mathrm{II}}(s)\,\mathrm{d}\overline{x}\,\mathrm{d}s,$$

$$\overline{c}_{35}=\overline{c}_{53}=-\frac{6\pi}{E'wh}\int_0^{\overline{\alpha}}sF_2(s)F_{\mathrm{II}}(s)\,\mathrm{d}s,$$

$$\overline{c}_{36}=\overline{c}_{63}=\begin{cases}\dfrac{2\pi}{E'\alpha'\xi A}\int_0^{\overline{\alpha}}\int_0^{1/2}s\overline{x}F_{\mathrm{II}}^2(s)\mathrm{d}\overline{x}\,\mathrm{d}s & (w\geq\sqrt{2}h),\\ \dfrac{2\pi}{E'\alpha' w^2}\int_0^{\overline{\alpha}}\int_0^{1/2}s\overline{x}F_{\mathrm{II}}^2(s)\,\mathrm{d}\overline{x}\,\mathrm{d}s & (w<\sqrt{2}h),\end{cases}$$

$$\overline{c}_{44}=\frac{18\pi}{E'w^3}\int_0^{\overline{\alpha}}\int_0^{1/2}\overline{x}sF_1^2(s)\,\mathrm{d}\overline{x}\,\mathrm{d}s,$$

$$\overline{c}_{45}=\overline{c}_{54}=\frac{36\pi}{EAw}\int_0^{\overline{\alpha}}\int_0^{1/2}\overline{x}sF_1(s)F_2(s)\,\mathrm{d}\overline{x}\,\mathrm{d}s,$$

$$\overline{c}_{46}=\overline{c}_{64}=\begin{cases}\dfrac{-6\pi}{E'\alpha'\xi w^2 h}\int_0^{\overline{\alpha}}\int_0^{1/2}s\overline{x}^2F_1(s)F_{\mathrm{II}}(s)\,\mathrm{d}\overline{x}\,\mathrm{d}s & (w\geq\sqrt{2}h),\\ \dfrac{-6\pi}{E'\alpha' w^3}\int_0^{\overline{\alpha}}\int_0^{1/2}s\overline{x}^2F_1(s)F_{\mathrm{II}}(s)\,\mathrm{d}\overline{x}\,\mathrm{d}s & (w<\sqrt{2}h),\end{cases}$$

$$\overline{c}_{55}=\frac{36\pi}{EAh}\int_0^{\overline{\alpha}}sF_2^2(s)\,\mathrm{d}s,$$

$$\bar{c}_{56}=\bar{c}_{65}=\begin{cases}-\dfrac{12\pi}{E'\alpha'\xi Ah}\int_0^{\bar{\alpha}}\int_0^{1/2}s\bar{x}F_2(s)F_{\mathrm{II}}(s)\,\mathrm{d}\bar{x}\,\mathrm{d}s & (w\geqslant\sqrt{2}h),\\ -\dfrac{12\pi}{E'\alpha'Aw}\int_0^{\bar{\alpha}}\int_0^{1/2}s\bar{x}F_2(s)F_{\mathrm{II}}(s)\,\mathrm{d}\bar{x}\,\mathrm{d}s & (w<\sqrt{2}h),\end{cases}$$

$$\bar{c}_{66}=\begin{cases}\dfrac{2\pi}{E'\alpha'Ah}\int_0^{\bar{\alpha}}\int_0^{1/2}s\left(\dfrac{1}{\xi}\bar{x}^2F_{\mathrm{II}}^2(s)+\dfrac{m}{4}F_{\mathrm{III}}^2(s)\right)\mathrm{d}\bar{x}\,\mathrm{d}s & (w\geqslant\sqrt{2}h),\\ \dfrac{2\pi}{E'\alpha'w^3}\int_0^{\bar{\alpha}}\int_0^{1/2}s\left(\bar{x}^2F_{\mathrm{II}}^2(s)+\dfrac{m}{4\xi}F_{\mathrm{III}}^2(s)\right)\mathrm{d}\bar{x}\,\mathrm{d}s & (w<\sqrt{2}h),\end{cases}$$

$$\bar{c}_{12}=\bar{c}_{21}=\bar{c}_{23}=\bar{c}_{32}=\bar{c}_{24}=\bar{c}_{42}=\bar{c}_{25}=\bar{c}_{52}=0, \tag{8}$$

where A is the area of the cross-section of the beam, $\bar{\alpha}=\alpha\sqrt{2}/(2h)$, $\bar{x}=x/w$.

The total flexibility of the cracked element can be obtained as $[\mathbf{C}_c]=[\overline{\mathbf{C}}]+[\mathbf{C}_0]$. $[\mathbf{C}_0]$ is the total flexibility matrix of the beam without crack, which can be derived by neglecting shearing action and by using the strain energy [20].

$$[\mathbf{C}_0]=\begin{bmatrix}l/AE & 0 & 0 & 0 & 0 & 0\\ 0 & l^3/3EI_x & 0 & 0 & l^2/2EI_x & 0\\ 0 & 0 & l^3/3EI_y & -l^3/2EI_y & 0 & 0\\ 0 & 0 & -l^2/2EI_y & l/EI_y & 0 & 0\\ 0 & l/2EI_x & 0 & 0 & l/EI_x & 0\\ 0 & 0 & 0 & 0 & 0 & l/GJ\end{bmatrix}, \tag{9}$$

where A is the area of the cross-section of the beam, l is the element length. Using the principle of virtual work, the stiffness matrix of the cracked element can be written as

$$[\mathbf{K}_{ec}]=[\mathbf{T}][\mathbf{C}_c]^{-1}[\mathbf{T}]^{\mathrm{T}}, \tag{10}$$

where $[\mathbf{T}]$ is the transformation matrix

$$[\mathbf{T}]^{\mathrm{T}}=\begin{bmatrix}-1 & 0 & 0 & 0 & 0 & 0 & 1 & 0 & 0 & 0 & 0 & 0\\ 0 & -1 & 0 & l & 0 & 0 & 0 & 1 & 0 & 0 & 0 & 0\\ 0 & 0 & -1 & 0 & -l & 0 & 0 & 0 & 1 & 0 & 0 & 0\\ 0 & 0 & 0 & -1 & 0 & 0 & 0 & 0 & 0 & 1 & 0 & 0\\ 0 & 0 & 0 & 0 & -1 & 0 & 0 & 0 & 0 & 0 & 1 & 0\\ 0 & 0 & 0 & 0 & 0 & -1 & 0 & 0 & 0 & 0 & 0 & 1\end{bmatrix}.$$

5.3. Application example

In order to validate the current crack element and the approach for cracked crankshaft model, an imitated crankshaft (not an actual crankshaft) including a crack is applied. Fig. 5(a) shows the finite element model meshed by solid elements, and a slant crack is contained in the left crank web. The total of elements is 8646, and the total of nodes is 16,428. Fig. 5(b) shows the model meshed by the current cracked element and 3-node Timoshenko beams. The total of elements is 14, the total of nodes is 28, and the element 5 is a crack beam element. The dimensions of the beam elements are listed in Table 5.

The influences of the crack depth on the natural frequencies of the two models are calculated respectively, the results of first four natural frequencies are shown in Fig. 6.

From Fig. 6, it can be seen that the natural frequencies of the two models are approximate, and the changes due to the crack depth are coincident in the rough. It is well known that solid finite element

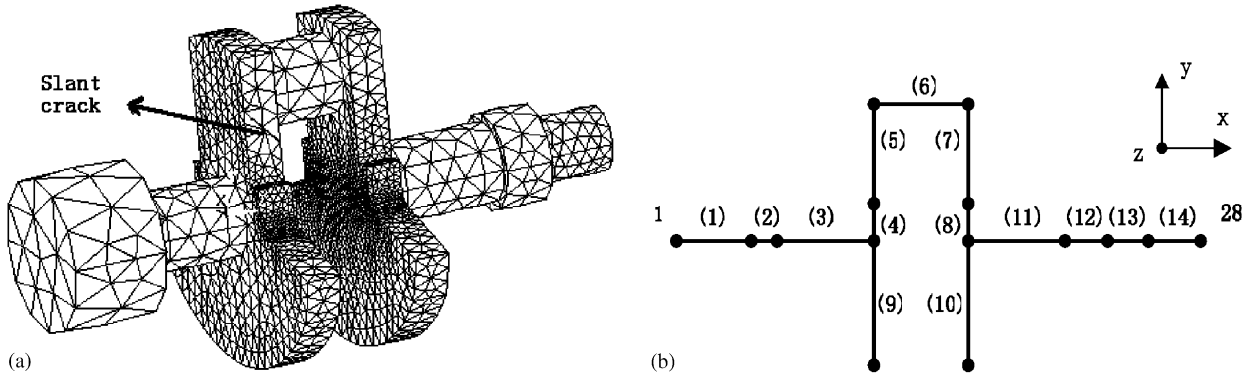

Fig. 5. The models of the imitated crankshaft (a) The solid element model; (b) the beam element model.

Table 5
Element dimensions and the members they represent in Fig. 5(b)

Element	1	2	3, 11	5, 7	6	4, 8	9, 10	12	13	14
Dimension (mm)	$\phi 96 \times 60.5$	$\phi 50 \times 10$	$\phi 50 \times 66$	$92 \times 26 \times 25$	$\phi 53 \times 72$	$72 \times 25.5 \times 50$	$180 \times 22 \times 90$	$\phi 50 \times 22$	$\phi 60 \times 30$	$\phi 40 \times 45$

method is robust for vibration analysis of structure, such that the application proves that the current crack beam element and the approach for cracked crankshaft model are valid for the vibration analysis of cracked crankshaft.

6. Nonlinear equation of motion

In order to find the dynamic response of the crankshaft-bearing system, the rotating crankshaft must be analyzed by combining with the non-rotating (fixed) main bearing. A common coordinate system is required for the combined model. For this reason, the analysis is performed with respect to a right-handed rotating coordinate system (X, Y, Z) that is attached to the crankshaft (see Fig. 7). The X coordinate is along the crankshaft axis towards the flywheel end and the Y coordinate point always to crankpin. The dynamic analysis described in this report assumes that the mass matrix $[M]$ of crankshaft system is time invariant.

Let the rotating speed of the crankshaft be ω, the angle between the initial position and the coordinate origin (x, y, z) be 0 (i.e., when $t = 0$, system (X, Y, Z) is superposed with system (x, y, z)). Therefore, under the rotating coordinate system the supporting stiffness $[\mathbf{K}^a]$ is

$$[\mathbf{K}^a] = \begin{bmatrix} K_{YY} & K_{YZ} \\ K_{ZY} & K_{ZZ} \end{bmatrix} = [\mathbf{T}']^{\mathrm{T}} \begin{bmatrix} k_{yy} & 0 \\ 0 & k_{zz} \end{bmatrix} [\mathbf{T}'], \tag{11}$$

where

$$[\mathbf{T}'] = \begin{bmatrix} \cos(\omega t) & -\sin(\omega t) \\ \sin(\omega t) & \cos(\omega t) \end{bmatrix}.$$

If $k_{yy} = k_{zz}$, then $K_{YZ} = K_{ZY} = 0$ and $K_{YY} = K_{ZZ} = k_{yy} = k_{zz}$. Combining $[\mathbf{K}^a]$ and the stiffness matrix of crankshaft body, the total stiffness matrix $[\mathbf{K}]$ of the operating crankshaft- bearing system can be yielded.

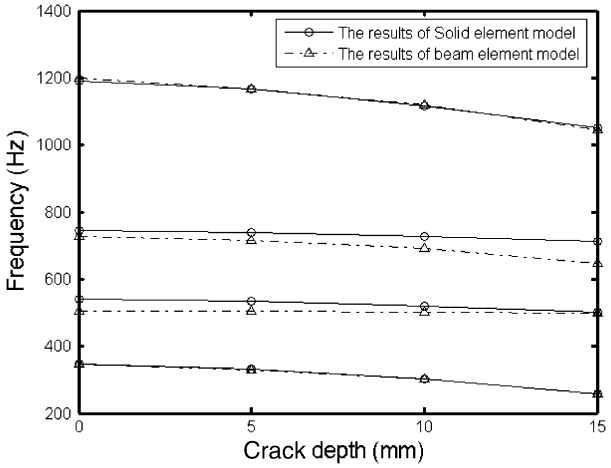

Fig. 6. The natural frequencies of the two models versus crack depth.

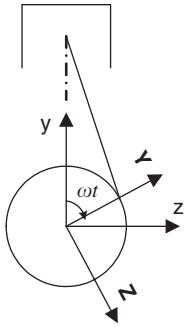

Fig. 7. Rotating coordinate system.

6.1. Modeling of breathing crack

In the operating condition, the crankshaft endures a cyclical impulsive load and the crack in crank web will be open and close (i.e., breathing). In this study, only fully open or fully closed conditions of crack are considered. When the crack is fully closed, the crankshaft will be treated as uncracked, the total stiffness of crankshaft-bearing system is $[\mathbf{K}_a]$. In other cases the crack will be treated as fully open, the total stiffness of cracked crankshaft-bearing system is $[\mathbf{K}_b]$. For the crack beam element shown in Fig. 8, let θ be the rotation displacement due to the bending moment M in x-y plane. Then the crack is open or closed according to the sign of the relative rotation $\Delta\theta$ ($\Delta\theta = \theta_j - \theta_i$) between nodes i and j, i.e., it is evaluated if the stresses in the cracked section are of tension or compression according to the bending moment that is applied at this cross-section. Then, the equation of motion that governs the dynamic behavior of the crankshaft-bearing system with a crack can be represented as expression:

$$[\mathbf{M}]\{\ddot{\mathbf{U}}\} + [\mathbf{D}]\{\dot{\mathbf{U}}\} + [\mathbf{K}(\Delta\theta)]\{\mathbf{U}\} = \{\mathbf{F}(t)\}, \tag{12}$$

where

$$[\mathbf{K}(\Delta\theta)] = \begin{cases} [\mathbf{K}_a] & \Delta\theta > 0 \quad \text{(crack is closed)}, \\ [\mathbf{K}_b] & \Delta\theta \leqslant 0 \quad \text{(crack is open)}, \end{cases}$$

$[\mathbf{D}]$ is the damping of system, $\{\mathbf{F}(t)\}$ is the vector of load applied on the crankshaft, they will be discussed later.

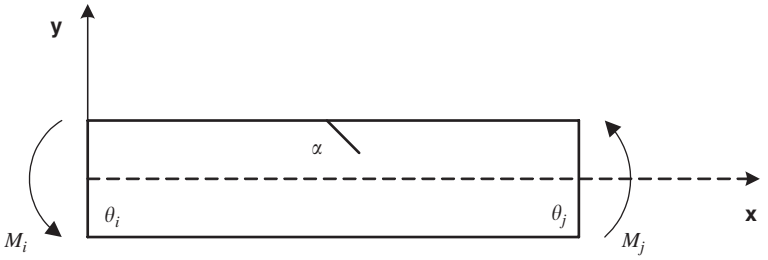

Fig. 8. Crack beam element.

6.2. Damping of crankshaft-bearing system

In the dynamic crankshaft-bearing system, there are two types of damping: hysteresis damping and oil film viscous damping. The oil film viscous damping is idealized by dashpots combined with linear springs mentioned above. The hysteresis damping $[\mathbf{D}^{\mathrm{H}}]$ is modeled as its viscous equivalent according to Raileigh distribution:

$$[\mathbf{D}^{\mathrm{H}}] = \alpha''[\mathbf{M}] + \beta''[\mathbf{K}(\Delta\theta)], \tag{13}$$

where α'' and β'' are two constants to be determined from two specified damping ratios which correspond to two unequal natural frequencies of the system. The following equation holds:

$$\alpha'' + \beta''\omega_i^2 = 2\zeta_i\omega_i, \tag{14}$$

where ω_i is the ith natural frequency of the system and ξ_i is the damping ratio for the ith mode. Given the natural frequencies and damping ratios of two different modes, the coefficients α'' and β''can be determined by solving Eq. (14).

6.3. Crankshaft loading

The crankshaft load is mainly comes from the cylinder combustion and the reciprocation inertia of the piston and connecting rod. This load is transmitted through the piston and connecting rod to the crankpin. The force F_c that acts on the crankpin is shown in Fig. 9. It can be resolved into the tangential force F_t and radial force F_r. The equivalent mass of the connection rod are treated as lumped mass and attached to crankshaft body. In the rotating coordinate system, the crankshaft inertia load due to centrifugal is equal to $m_1 r\omega^2$, where m_1 is the mass of the element, r is the distance of its center of gravity from the rotating axis of the crankshaft.

7. Simulation and result analysis

As the total load $\{\mathrm{F}(t)\}$ acted on the crankshaft is periodic, it can be expanded into a series of harmonic force components by Fourier analysis. Generally, the certain lower order harmonics force components have dominant impact and the higher order harmonics can be ignored.

In this section, simulation is conducted on the crankshaft shown in Fig. 2. Assuming that the rotating speed be 1500 r/min, the load is computed and resolved as the method described in Section 6.3, and the first 40 order components are kept after expansion. The resolved load acts on the surface of elements corresponding to crankpins in the four-stroke style. Thus, the excitation force consists of a series harmonics of $12.5n$ ($n = 0, 1, 2, \ldots, 40$), and the frequency band is from 0 to 500 Hz. Presume that the crack occurs in the element 16 shown in Fig. 2. The modeling procedures aforementioned are implemented to simulate the vibration analysis of the crankshaft including different relative depth crack of 0, 2%, 4%, 10%, 20% and 40%.

In practical experiments, the torsional and longitudinal vibration at the free end can be measured directly. The bending vibration of the main journal will transfer to the shell of engine block via the bearing supporting, so it is can be acquired indirectly. In general, these vibration signals are used to analyze the dynamic

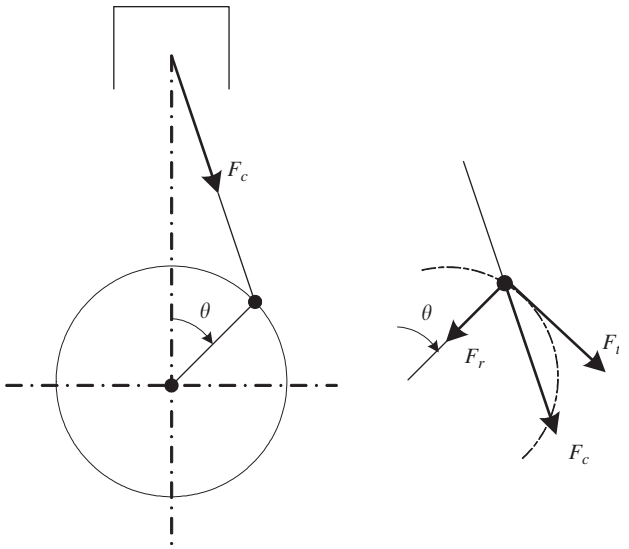

Fig. 9. Decomposition of the exciting force.

characteristics of the crankshaft. Therefore, only the results of the torsional and longitudinal vibration response of node 1, the bending vibration response of the mid-node in 3# main journal are presented and analyzed here. The corresponding frequency spectra are shown in Figs. 10–13.

Figs. 10(a)–(d) show the frequency spectra of the torsion of node 1 with different relative crack depth. In Fig. 10(a) the corresponding relative crack depths are 0%, 2% and 4%, respectively; the frequency range is from 0 to 50 kHz. In Figs. 10(b) and (c), the frequency ranges are 0–500 and 500–3000 Hz, respectively. Fig. 10(d) shows the frequency spectra of the torsion of node1 with deeper relative crack of 10%, 20% and 40%. Fig. 11 shows the frequency spectra of the longitudinal vibration acceleration of node 1. Fig. 12 and 13 show the frequency spectra of the bending vibration acceleration of the mid-node at 3# main journal with different crack depth, respectively. The former is in y direction, and the latter is in z direction.

In all these spectra (from Figs. 10 to 13), the following observations can be obtained: (1) The harmonic components higher than that of exciting force will appear in the vibration response due to crack; (2) the order of appeared higher harmonic components will be $n/2$ $(n = 1, 2, \ldots)$ times of the rotating frequency of crankshaft, the presence of these harmonic components is due to the nonlinearities; (3) the amplitudes of the higher harmonic peak and the distributing band of the higher harmonic components will increase with the crack depth increasing; (4) the amplitudes of components corresponding to the exciting force frequency is less sensitive to crack depth.

8. Conclusions

In this work, a new method for simulating nonlinear motion of cracked crankshaft is proposed and the transient vibration response of a cracked crankshaft is analyzed. The main contents and conclusions are as follows.

1. A finite element model based on 3-node Timoshenko beam element for crankshaft-bearing system is proposed. The comparison between the analytical and experimental results of vibration modes indicates that the proposed model is effective.
2. The stiffness matrix of a new slant crack beam element is developed, and it can be applied widely to any structure including such a slant crack.
3. The cracked crank web is idealized as the developed crack beam element, and a new model for the vibration analysis of cracked crankshaft is established. Evidently, such cracked crankshaft model is easy to establish and computationally effective to implement.

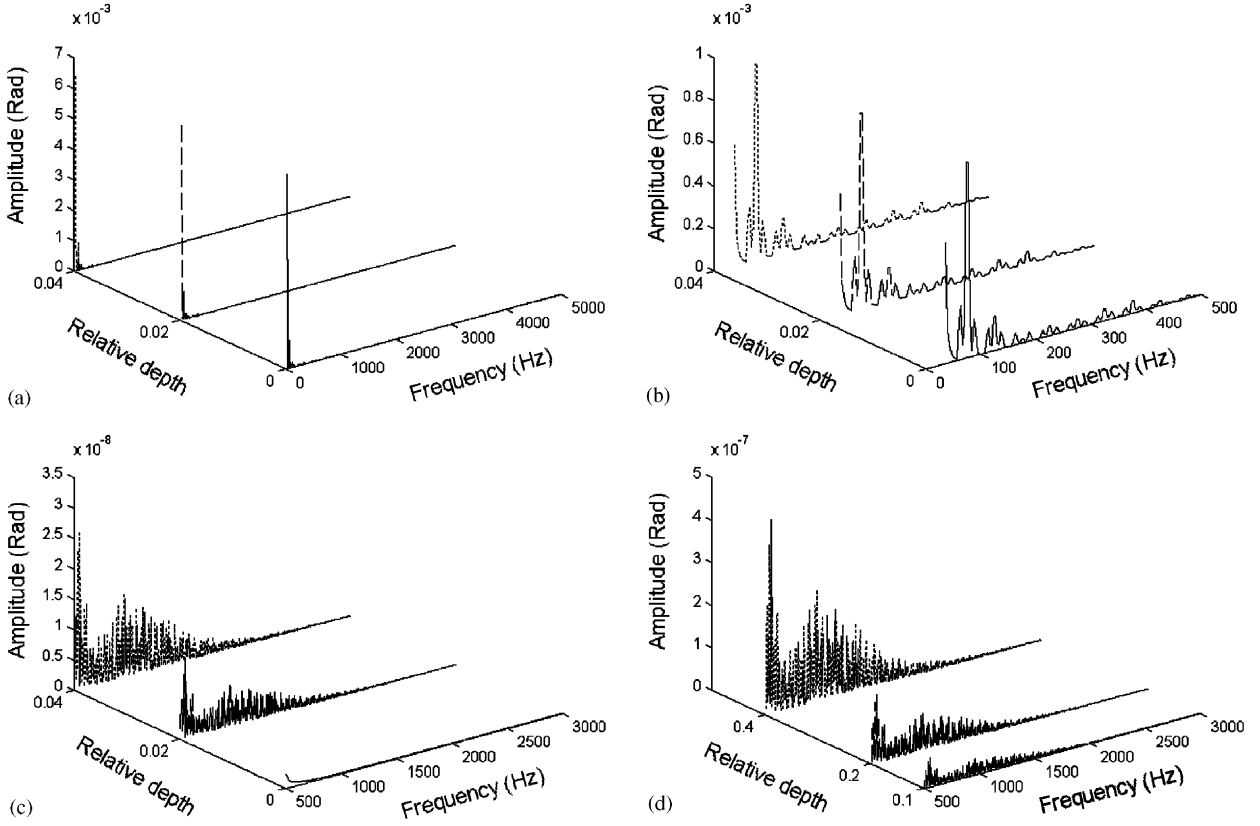

Fig. 10. Frequency spectra of torsional vibration of node 1 with relative crack depths (a) All harmonic frequencies; (b) lower harmonic frequency components in (a); (c) the harmonic frequency from 500–3000 components in (a); (d) the harmonic frequency components with deeper crack.

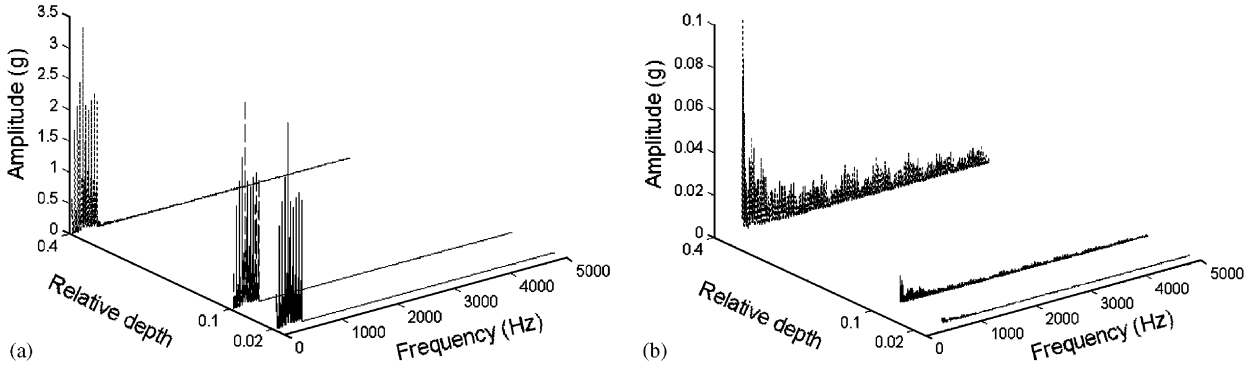

Fig. 11. Frequency spectra of longitudinal vibration of node 1 with relative crack depths (a) All harmonic frequencies; (b) higher harmonic frequency components in (a).

4. The transient vibration response of a certain cracked crankshaft is calculated and analyzed, and some conclusions are drawn from the results. However, these conclusions will be validated in further work.

This work provides a useful tool for the vibration analysis and crack detection of cracked crankshaft system.

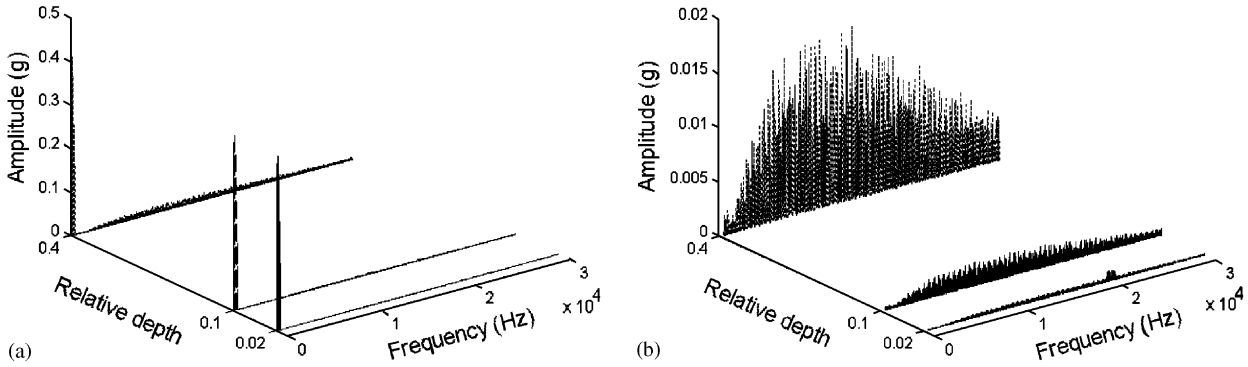

Fig. 12. Frequency spectra of bending vibration in y direction of the mid-node in 3# main journal with relative crack depths (a) All harmonic frequencies; (b) higher harmonic frequency components in (a).

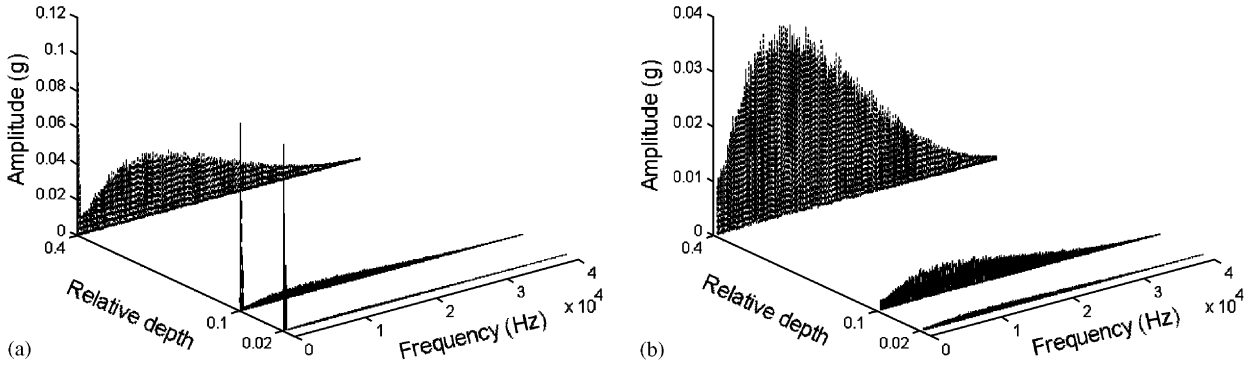

Fig. 13. Frequency spectra of bending vibration in z direction of the mid-node in 3# main journal with relative crack depths (a) All harmonic frequencies; (b) higher harmonic frequency components in (a).

Acknowledgment

This work has been supported by the National Natural Science Foundation (Approved Grant: 10176014) and the National Natural Science Foundation of China (No. 50335030).

References

[1] Lihua Xu, On several key problem of shipping engine, *Wuhan Ship Building* 133 (4) (2000) 19–23.
[2] R.K. Pandey, Failure of diesel-engine crankshafts, *Engineering Failure Analysis* 10 (2) (2003) 165–175.
[3] T. Sofronas, Analyzing a crankshaft failure, *Hydrocarbon Processing* 82 (4) (2003) 89.
[4] D. Taylor, A.J. Ciepalowicz, P.I. Rogers, et al., Prediction of fatigue failure in a crankshaft using the technique of crack modeling, *Fatigue and Fracture of Engineering Materials & Structures* 20 (1) (1997) 13–21.
[5] M. Guagliano, L. Vergani, Simplified approach to crack growth prediction in a crankshaft, *Fatigue and Fracture of Engineering Materials & Structure* 17 (11) (1994) 1295–1306.
[6] Miyahara Mitsuo, Nomoto Kenichi, Umino Masahide, et al., Development of life prediction model and improvement of a die steel for hot forging die, *Sumitomo Metals* 48 (2) (1996) 76–84.
[7] H. Wang, L.-T. Yan, Q.-H. Li, Diagnosis of crankshaft cracks via the measurement of the torsional modal characters of a crankshaft flywheel system, *Proceedings of the First International Machinery Monitoring and Diagnosis*, 1989, pp. 340–345.
[8] W. Schiffer, J. Jenzer, 3-D shafting calculations for marine installations: static and dynamic, *American Society of Mechanical Engineers, Internal Combustion Engine Division (Publication) ICE* 40 (2003) 297–303.

[9] Cui Zhiqin, Xu Yangfang, Modal analysis on the combined structure of engine, *Proceedings of the International Symposium on Test and Measurement* 4 (2003) 3170–3172.
[10] H. Okamura, A. Shinno, T. Yamanaka, K. Sogabe, Simple modeling and analysis for crankshaft three-dimensional vibrations—part 1:background and application to free vibrations, *Journal of vibration and acoustics* 117 (1995) 70–79.
[11] H.H. Priebsch, J. Affenzeller, S. Gran, Prediction technique for stress and vibration of nonlinear supported, rotating crankshafts, *Journal of Engineering for Gas Turbines and Power, Transactions of the ASME* 115 (4) (1993) 711–719.
[12] S.S. Rao, *The Finite Element Method in Engineering*, Pergamon Press, Oxford, 1989.
[13] A.A. Smaili, M.P. Khetawat, Dynamic modeling of automotive engine crankshafts, *Mechanism & Machine Theory* 29 (7) (1994) 995–1006.
[14] V. Yildirim, E. Kiral, Investigation of the rotary inertia and shear deformation effects on the out-of-plane bending and torsional natural frequencies of laminated beams, *Composite Structures* 49 (2000) 313–320.
[15] Y.K. Cheung, D. Zhou, Vibrations of moderately thick rectangular plates in terms of a set of static *Timoshenko* beam functions, *Composite Structures* 78 (2000) 757–768.
[16] Zhong Shilian, Liu Dunkang, Calculation measure on the stress at the inner corner of compressor crankshaft, *Liu Ti Jixie* 27 (6) (1999) 11–15.
[17] C.A. Papadopoulos, A.D. Dimarogonas, Coupled longitudinal and bending vibrations of a rotating shaft with an open crack, *Journal of Sound and Vibration* 117 (1) (19876) 81–93.
[18] T.C. Tsai, Y.Z. Wang, Vibration analysis and diagnosis of a crack shaft, *Journal of Sound and Vibration* 192 (3) (1992) 607–620.
[19] P.N. Saavedra, L.A. Cuitino, Crack detection and vibration behavior of cracked beams, *Computer and Structures* 79 (2001) 1451–1459.
[20] A.S. Sekhar, Conditioning monitoring of a rotor system having a slant crack in the shaft, *Noise and vibration worldwide* 30 (3) (1999) 23–31.
[21] A.W. Lees, Fault diagnosis in rotating machinery, *Proceedings of the International Modal Analysis Conference—IMAC* vol. 1, 2000, pp. 313–319.
[22] Lei Xuanyang, Song Xigeng, New model for 3-D vibration of internal combustion engine crankshaft, *Zhongguo Jixie Gongcheng* 14 (17) (2003) 1466–1470.
[23] J.N. Sundermeyer, R.L. Weaver, On crack identification and characterization in a beam by non-linear vibration analysis, *Journal of Sound and Vibration* 183 (5) (1995) 857–871.
[24] H. Tada, P.C. Paris, G.R. Irwin, *The Stress Analysis of Crack Handbook*, Del Research Corp., Hellertown, PA, 1973.